PAPER

Check for updates

Crack opening: from colloidal systems to paintings

Marguerite Léang, [ID] *[ab] Frédérique Giorgiutti-Dauphiné,[a] Lay-Theng Lee[b] and Ludovic Pauchard [ID] [a]

Shrinkage cracks are observed in many materials, particularly in paintings where great interest lies in deducing quantitative information on the material with the aim of proposing authentication methods. We present experimental measurements on the crack opening induced by the drying of colloidal layers and compare these results to the case of a pictorial layer. We propose a simple model to predict the crack width as a function of the thickness of the drying layer, based on the balance between the drying stress buildup and the shear frictional stress with the substrate. Key parameters of the model include the mechanical properties that are measured experimentally using micro-indentation testing. A good agreement between theory and experimental data for both colloidal layers and the real painting is found. These results, by comparing the shrinkage cracks in model layers and in pictorial layers, validate the method based on the use of colloidal systems to simulate and to reproduce drying cracks in paintings.

1 Introduction

Differential shrinkage in a material may cause material cracking. Shrinkage can result from different causes: water removal from a particulate material, cooling or aging through a chemical process. From this shrinkage a wide range of patterns can result in many materials and particularly in art paintings. In this case, the great complexity and variety of crack pattern morphologies are a potential source of information on the materials used and the methods employed by the artists. Analysis of crack patterns may provide important clues to the mechanical properties, composition or implementation of the work of art[1] and consequently can help to authenticate paintings. It can be used to detect an "original crack pattern" from a "fake crack pattern" obtained by art forgers as an attempt to reproduce paintings.[2]

There are many possible classifications of crack patterns in the literature[3,4] which take into account the global features of the crack pattern as well as the features of an individual crack. The consensus concerns the type of single crack and where two typical cracks are defined: drying or premature cracks, and age cracks. The first type occurs during the first hours or days in the life of a painting whereas the second can appear after many years. Drying cracks result from mechanical stresses due to

chemical or physical drying and are usually confined to a single layer and do not penetrate into the sub-layers. Physical drying is induced by solvent removal, whereas chemical drying involves a chemical reaction between molecules (for example polymerization by the action of oxygen[5]). Concerning age cracks, they are due to environmental changes and appear when the material can no longer withstand the stress due to its embrittlement from chemical or physical alterations. One of the easiest ways to distinguish between these two types of cracks is to observe their specific widths. In particular, the width of drying cracks due to a drying process is in most cases greater than those due to aging. As an example, such a typical crack pattern is presented in Fig. 1 in the painting by Louis Crignier. The enlargement of the painting showing the shoulder of "Jeanne d'Arc" highlights a drying crack pattern where the opening of the crack is so significant that it reveals the sub-layer. The rate of shrinkage and consequently the width of a crack depends on the mechanical properties of the material.

Numerous works deal with crack patterns, for example to study the nucleation of cracks, to distinguish between various morphologies of the resulting cracks or to study the crack spacing, in various systems and on different scales.[6] Nevertheless, only a few deal with crack widths. Lecocq et al.[7] studied the dynamics of the crack opening in drying clay and they proposed a simple model to recover the increase of the crack opening with time. Some works focus on the crack propagation between two materials.[8,9] Generally, the shear stress at the interface is expressed through a linear viscous friction law such that the shear stress is proportional to the sliding velocity. In a

[a] Laboratoire F.A.S.T, UMR 7608 CNRS - Univ. Paris-Sud, Université Paris-Saclay, 91405, Orsay CEDEX, France. E-mail: leang@fast.u-psud.fr

[b] Laboratoire Léon Brillouin, UMR 12 CEA-CNRS, CEA Saclay, 91191, Gif-sur-Yvette CEDEX, France
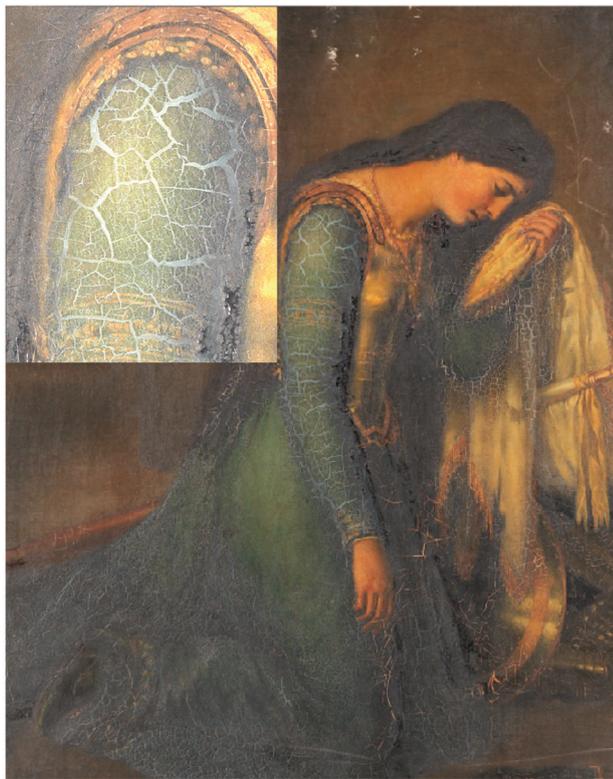
Fig. 1 Photograph in visible light of the painting "Jeanne d'Arc en prison" by Louis Crignier (1824) – 1164 × 885 mm – Musée de Picardie, Amiens, ©C2RMF/A. Maigret. Inset: Detail of the shoulder showing a drying crack pattern.

multilayered system, this is a complicated problem as it depends mainly on the ability of the material to mechanically resist shrinkage and on the possibility of the sliding of one layer on the sublayer.

In the present paper, we study the width of drying cracks observed in aqueous suspensions of silica nanoparticles and we compare our results with measurements on a painting. We focus on the width of the first generation of cracks as the crack pattern results from the successive formation of cracks.[10] Each individual crack modifies the mechanical stress field in its vicinity, modifying the crack path of the successive crack. In this way, each generation of crack spatially affects the next one. The first generation of cracks, as formed in the less consolidated material, displays the largest crack opening.

We measure the crack width and its dependence on the thickness of the drying film in three different systems and on a real painting. A scaling law is then deduced to fit the experimental results based on a balance between the friction with the substrate and the shrinkage due to the drying expressed through the theory of poroelasticity.[11] The parameters of this model are evaluated experimentally using indentation testing measurements and a friction coefficient between the layer and its sub-layer is deduced. Similar behaviors are observed between model systems and paintings which validate the use of colloidal suspensions to model crack patterns in paintings.

2 Experiments and models

2.1 Systems

A paint layer is a complex system made of a binding medium and pigments and various additives to enhance the deposition and the consistency of the paint layer. A generic formulation is difficult to establish. Therefore our model system based on silica nanoparticles is not meant to depict the large variety of behaviors encountered in real paintings, but aims to reproduce the morphologies observed in real paintings in a more controllable system.[1]

Pigments are mainly responsible for the mechanical properties of a pictorial layer. They exhibit specific mechanical properties and surface roughness that depend on the material and the way they were ground. In particular, a realistic value for the mean surface roughness is 10 nm according to Petit *et al.*[12] As the roughness defines the smallest characteristic length of the system, it controls the transport of fluid in the consolidated material and hence the increase of the drying stress. Therefore, we investigate aqueous suspensions of silica nanoparticles as model systems with a particle size of the same order of magnitude of the pigment roughness: Ludox SM-30, HS-40 and TM-50 purchased from Sigma-Aldrich. The main properties of these systems are reported in Table 1. In the absence of evaporation the stability of the dispersions is ensured by a competition between van der Waals attraction and electrostatic repulsion according to the DLVO theory.[13] Surface tensions of the dispersions fall in the range (57; 67) mN m^{-1} and the particle size polydispersity is ~ 0.18.

2.2 Methods

For each system, an initial volume of silica dispersion is deposited on a circular glass Petri dish, and left to dry at ambient temperature and relative humidity RH $\sim$ 50%. The drying conditions are characterized by the evaporation rate, V_E. This evaporation rate is measured by mass variations of a sample, and the characteristic drying time h/V_E for a layer of thickness h varies from several minutes to a week, depending on the initial volume deposited. The Petri dishes are previously cleaned with 5% Decon in distilled water and ethanol, and then dried at 100 °C. This specific cleaning protocol ensures reproducible conditions of adhesion between the colloidal layer and the substrate. Upon drying, particles

Table 1 Main characteristics of the colloidal dispersions used in the experiments: a: mean particle radius; ϕ_0: initial volume fraction. Measurements of the mechanical properties using indentation testing (measurements performed 10 minutes after the formation of the crack pattern): E: elastic modulus; σ_Y: yield stress (elastic modulus and yield stress for model systems are estimated through statistics on measurements performed using indentation testing under the same conditions); t_y: time to reach the yield point

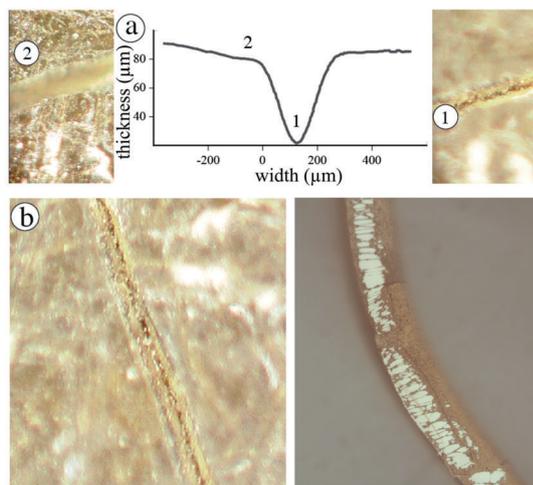| Silica dispersions	2a (nm)	ϕ_0	Solid gels	E ($\times 10^8$ Pa)	σ_Y ($\times 10^7$ Pa)	t_y ($\times 10^2$ s)
SM-30	10	0.15	SM-30	4.4 ± 0.8	2.4 ± 0.6	1.04
HS-40	16	0.19	HS-40	4.0 ± 0.8	2.2 ± 0.6	1.06
TM-50	26	0.30	TM-50	3.4 ± 0.8	1.4 ± 0.6	0.79
Pictorial	—	—	Pictorial	3.4	1.4 $\pm$ 0.8	

Fig. 2 (a) Crack profile measured through differential focusing using a 3D digital video microscope Hirox for the painting "Jeanne d'Arc en prison"; image 1 is focused at the bottom of the crack profile; image 2 is focused at the surface of the paint layer. (b) The crack opening extends to the sublayer. At left the image is focused on the sublayer surface of a region of the painting "Jeanne d'Arc en prison": the dark jagged line corresponds to the crack path in the sublayer. At right the same process can be observed in a model system made of stratified layers; the sublayer exhibits thin wires in the direction of the tensile force (image width: 500 μm). Due to solvent removal, large stresses develop resulting in the formation of a hierarchical crack pattern. In most cases the different generations of cracks are unambiguously identifiable.

concentrate and form a solid layer of approximately constant thickness in the center of the dish. The thickness of the solid layer is controlled by the volume of dispersion initially deposited. The local thickness of the solid layer is measured using an optical microscope (objective ×10, DM2500 Leica optical microscope) by transmitted light, focalizing on the surface of the layer and on the surface of the glass Petri dish. In the case of the pictorial layer, a 3D digital video microscope (Hirox) is used to measure the surface topography. Moreover this method allows us to measure precisely the layer thickness using differential focusing throughout a crack (see Fig. 2a).

The crack widths, w, for the first generation (Fig. 3a) are measured at different locations on the same sample and repeated on different samples, to deduce an average value. The measurements are done in the center of the Petri dish in order to avoid evaporation inhomogeneity due to boundary conditions. They are performed on different thicknesses using three colloidal systems of different particle sizes.

Measurements of the mechanical properties are performed using a MHT-CSM Instruments Micro Indentation Testing[14,15] with a spherical indenter of radius R = 0.25 mm (Fig. 4). The solid layers are about 1 mm thick deposited on a rigid glass slide. Indentation measurements were performed on solid fragments just after the formation of the first cracks during the CRP (constant rate period[16]). Each measurement starts as soon as the final crack pattern does not evolve anymore. Starting with the indenter in contact with the surface of the solid film, the spherical tip is driven inside the sample with a loading speed of 100 mN min^{-1} until a maximum load F_m = 100 mN is reached.
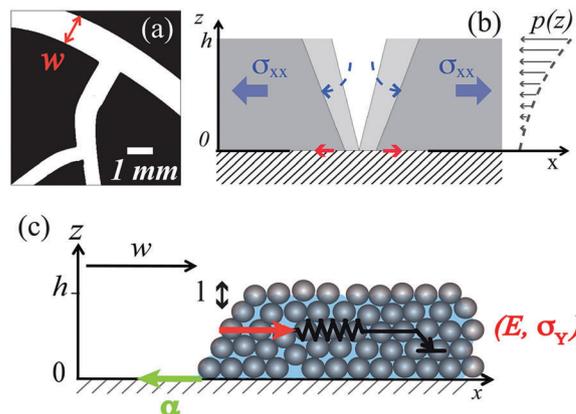

Fig. 3 (a) Width, w, of a crack path corresponding to a first generation. (b) Distribution of the pressure in the liquid pores along the porous layer thickness; the drying stress, σ_{xx}, results in the opening of a crack (here a fully penetrating crack). (c) Sketch of the side view of a single fragment subjected to elastic and friction forces during the drying process. The physical system is characterized by the elastic modulus, E, the yield stress, σ_Y, of the material, and the frictional parameter, α.
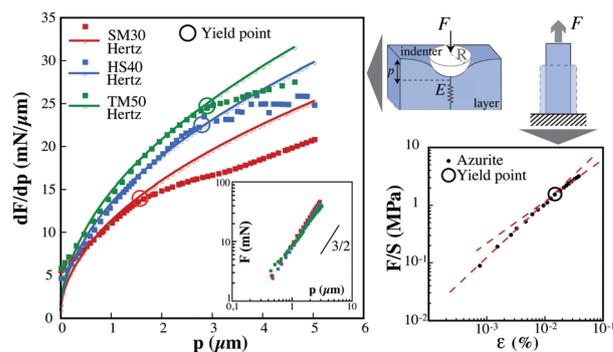

Fig. 4 Mechanical properties of three colloidal layers and one pictorial layer. Left: Comparison between purely elastic indentation curve and elastic–plastic indentation curve for layers made of dried TM-50, HS-40, and SM-30 Ludox dispersions. The derivative of the applied load, dF/dp, with respect to the penetration depth, p, is plotted as a function of p. Squares correspond to measurements while solid lines correspond to a purely elastic model according to the Hertz law. The yield point is indicated by the circle corresponding to the deviation from the Hertz law. Inset: Evolution of the load force F as a function of depth penetration p in the material. Right: The uniaxial tensile stress–strain curve of an elastic–plastic material; the yield point is indicated by the circle. Data extract from Mecklenburg et al.[19] for azurite in cold pressed linseed oil, for relative humidity RH ∼ 50% for 7.5 years.

Note that the choice of the value of F_m is such that the external pressure exerted by the tip, F_m/S (S being the projected surface of the tip on the film), is close to the capillary pressure $|P_{cap}| \sim 10^8$ Pa exerted by the air/solvent meniscus at the evaporation surface of the layer.[16] The applied force, F, is then measured as a function of the penetration depth, p, in the material (see schema in Fig. 4). Measurements are well fitted by the Hertz contact law over a range of indentation depths limited to the purely elastic case within the limits of small deformation.[17] Thus:

$$F = \frac{4\sqrt{R}}{3(1 - \nu^2)} E p^{3/2} \tag{1}$$

where ν being the Poisson ratio of the layer (we use the value $\nu = 0.2$[18]). The derivative of the applied load with respect to the penetration depth is plotted for the three solid systems in Fig. 4.

3 Model

The successive processes responsible for the crack pattern formation and evolution are depicted in Fig. 3. Upon drying, large stresses build up in the gel layer and cause layer shrinking. We assume that the atmospheric pressure ($\sim 10^5$ Pa) is negligible compared with the capillary pressure (up to 10^8 Pa) that arises during drying. Thus the stress tensor is mainly in the plane of the layer and we will only consider the components σ_{xx} and σ_{yy} in the following. In particular, in a newly fractured layer, the drying stresses result in the crack shape evolution.

One should note that there is a critical thickness h_c below which layers are usually crack-free, since the elastic energy stored in the material is insufficient to propagate cracks.[20,21] This critical value is given by: $h_c = \frac{EG_0}{0.6\pi\sigma^2}$ with G_0, the energy release rate and σ, the stress which is taken to be equal to the capillary pressure. This critical thickness is then equal to 0.6 µm in our systems. Evidence for this critical thickness can be seen in Leonardo da Vinci's paintings where the artist succeeded in applying very thin (of the order of a few micrometers) paint layers which avoid cracking (technique of Sfumato).[1] In the following, the opening of cracks is investigated in layers thicker than 1 µm.

The shrinkage process results from the variation of liquid pressure in the pore liquid as: $\sigma_{xx}(z,t) = \sigma_{yy}(z,t) = \frac{1-2\nu}{1-\nu}(p_0 - p(z,t))$, where p_0 is the initial pressure corresponding to the unstressed material, and $p(z,t)$ is the local value of the pressure in the liquid pore at time t and height z in the porous layer. Therefore, the quantification of drying stress requires a theory of coupling fluid dynamics and solid mechanics, which is the theory of poroelasticity. In the gel phase, the pressure distribution in the liquid pores satisfies the following differential equation:[11]

$$\frac{\partial p}{\partial t} = D_p \frac{\partial^2 p}{\partial z^2} \qquad (2)$$

where $D_p = \frac{kE}{\eta}$ is the diffusivity, also called the consolidation coefficient, E is the elastic modulus of the gel, η is the viscosity of the fluid and k the permeability of the porous gel. An analytical solution of eqn (2) is given in ref. 22–24. Together with the boundary condition at the upper surface of the film, $\frac{\partial p}{\partial z}\Big|_{z=h} = -\frac{V_E\eta}{k}$, the spatial and time variations of the pore pressure $p(z,t)$ are calculated. The distribution of pressure over the layer thickness is illustrated in Fig. 3b. At the upper surface of the drying gel, the highest value of the liquid pressure leads to drying stress: $\sigma_{xx}(z = h, t) = \frac{1-2\nu}{1-\nu}\left(\left(p_0 + \frac{hV_E\eta}{3k}\right) + \frac{V_EE}{h}t\right)$.

The second term of this equation is much larger than the first one as a result of the surface evaporation surpassing the flow inside the porous layer. Thus it becomes:

$$\sigma_{xx}(z = h, t) \sim \frac{1-2\nu}{1-\nu}\left(\frac{V_EE}{h}t\right) \qquad (3)$$

However the drying stress does not increase indefinitely with time as predicted by eqn (3) since a plastic response is required during drying.[25] Basically, the yielding behaviour occurs at time t_Y such that: $\bar{\sigma}_{xx}(t_Y) = \sigma_Y$, where σ_Y is the yield stress of the material and $\bar{\sigma}_{xx}$ is the drying stress averaged over the thickness of the layer. It turns out that the integration of the stress over the thickness of the layer $\bar{\sigma}_{xx}(t)$ gives the value of the stress at the interface, so: $\bar{\sigma}_{xx}(t) = \sigma_{xx}(z = h, t) = \frac{1-2\nu}{1-\nu}EV_E\frac{t}{h} \sim EV_E\frac{t}{h}$. Using eqn (3), the limit of elasticity of the material is reached at:

$$t_Y = \frac{\sigma_Y}{E}\frac{h}{V_E} \qquad (4)$$

The strain induced by shrinkage is classically expressed as: $\varepsilon_{xx}(h,t) = \frac{p(h,t)}{K}$, where $K = E/3(1-2\nu)$ is the bulk modulus.[26] A simple calculation shows that the strain increases linearly with time as $\varepsilon_{xx}(h,t) \sim \frac{1}{3(1-2\nu)}\frac{V_E}{h}t$. In particular, this equation gives the time variation of the crack width in a drying colloidal gel. The largest value reached by the strain occurs at $t = t_Y$ and is expressed:

$$\varepsilon_{xx}(h, t_Y) \sim \frac{1}{3(1-2\nu)}\frac{\sigma_Y}{E} \qquad (5)$$

The penetration depth of cracks in a layer can then be estimated by balancing the elastic strain energy with the surface energy of the cracks. Assuming that most of the stress is concentrated in a layer of thickness l within the film (see Fig. 3c), the elastic energy per unit length is expressed as: $\frac{1}{2}E\varepsilon_{xx}^2lL$, where L is the mean crack spacing in the layer (see Fig. 5b). Since the drying stress reaches the maximum intensity at the evaporation surface, the length l is assumed to scale with the particle size.[27] The cracks extend throughout a penetration depth h' so that the surface energy is $2\Gamma h'$, where Γ is the energy dissipated during fracture per unit of a newly created fracture surface area. When the maximum strain is reached, using eqn (5), the maximum depth h_m' becomes:

$$h_m' \sim \left(\frac{\sigma_Y}{E}\right)^2\frac{ELl}{4\Gamma} \qquad (6)$$

Eqn (5) and (6) show that the ratio $\frac{\sigma_Y}{E}$ is the key parameter to determine the final crack pattern of the solid layer.

For a solid layer adhering to an infinitely stiff sublayer, cracks penetrate fully in the layer; however the crack does not affect mechanically the sublayer. In this case, the final crack width is due to a balance between the shrinkage process and the frictional process on the sublayer that limits the crack width. Since the adhesion between the colloidal layer and the
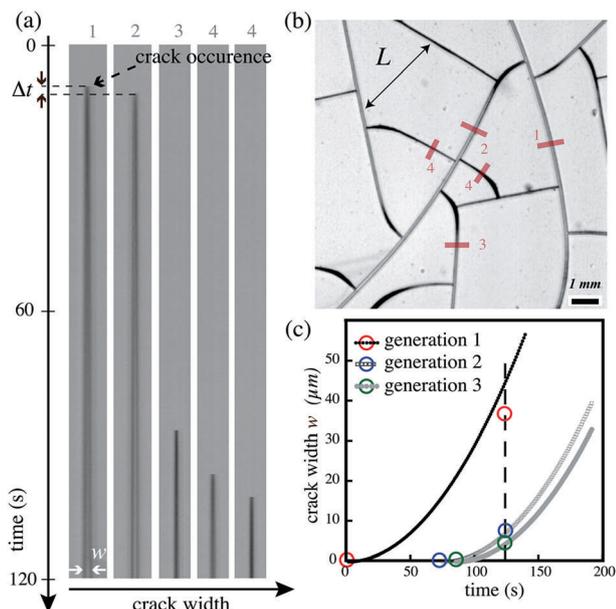
Fig. 5 (a) Successive spatiotemporal diagram corresponding to the successive generations of cracks in image (b). The crack generations are numbered from 1 to 4. (b) Hierarchical formation of a crack pattern in a layer of Ludox HS-40. L is the mean crack spacing in the layer. (c) Width of individual cracks of generation 1, 2, 3 with time; circles are measurements deduced from the spatiotemporal diagrams in (a).

sublayer is mainly governed by capillary bridges,[28] the frictional shear force with the substrate is assumed to be a linear viscous force such that: $\alpha dx/dt$ per unit length, where α (> 0, in Pa s) is the viscous friction parameter of the gel and dx/dt is the sliding velocity of the layer on the sublayer[7] (Fig. 3c). Therefore, assuming a quasi static process, a balance between the drying force and the frictional force with the substrate, per unit length, is expressed as:

$$\sigma_{xx}(z = h, t)l = \alpha dx/dt \qquad (7)$$

By integrating eqn (7), one finds a non-linear relation between the crack width and time in a purely elastic layer:

$$x(t) = \frac{1 - 2\nu}{1 - \nu}\frac{l}{2}\frac{V_E E}{h}\frac{1}{\alpha}t^2 \qquad (8)$$

Finally, at time t_Y the final crack width is reduced to:

$$w/h = \frac{1 - 2\nu}{1 - \nu}\frac{l}{2}\frac{\sigma_Y^2}{EV_E}\frac{1}{\alpha} \qquad (9)$$

We note that the drying stress is distributed unevenly in the vicinity of an open crack but we assume that this does not affect the simple model presented here.[29,30]

4 Experimental results

Fig. 5b shows a typical pattern of drying cracks exhibiting successive generations. As cracks are formed by successive generations, individual cracks usually do not exhibit identical width at the final stage of pattern formation. Indeed, a delay

time may exist between successive generations as shown by the spatiotemporal diagram corresponding to successive generations in Fig. 5a. In particular, the delay time, Δt, between generation 1 and 2 is only a few seconds while Δt reaches several tens of seconds between generation 2 and 3. Nevertheless, the mechanical properties of the layer are assumed to be unmodified during this period of time. This delay time can vary with the drying rate or the density of defects in the layer. As seen in Fig. 5b, the crack width decreases with the order of generation. The vertical dashed line in Fig. 5c corresponds to the time t_Y where the material gels and we assume that at that time, the material becomes plastic. The curves represent the time variation of the crack width according to the simple model depicted by eqn (8). Therefore, the measured crack width is the value corresponding to the intersection between the curve and the dashed line. The time variation for the width is assumed to be the same for all crack generations; they are simply shifted. Consequently the crack generation n should be thinner than the generation $n - 1$. When the layer behavior reaches the yield point, the evolution of the entire crack pattern is stopped, fixing the width of individual cracks. The yield point determines the final crack width of the crack pattern as shown by the equations obtained in Section 3. It is then essential to quantify the mechanical properties of the material, especially the elastic modulus and the yield stress that control the final crack width. These measurements are achieved by indentation testing (see Section 2.2). Under low applied force, the elastic response of the materials allows us to estimate the elastic modulus according to the Hertz contact law (Fig. 4). Results are reported in Table 1 for the three silica layers. However, above a critical applied force, the discrepancy with this Hertz law suggests that the material becomes plastic (Fig. 4). The critical penetration depth, p_c, provides the value for the yield stress as: $\sigma_Y = 0.434E\sqrt{p_c/R}$, according to ref. 17 and 31. Note that while p_c increases with particle size, the elastic modulus shows an opposite trend, resulting in a yield stress that is inversely proportional to the particle size (Table 1), as predicted[32] and obtained in the experimental measurements. The resulting timescale at which the yield point is reached is reported in Table 1.

Model systems

To test the validity of eqn (9), the widths of first generation cracks, w, have been measured and plotted in Fig. 6 for different silica layers, over a wide range of layer thickness $[10^{-5}; 10^{-3}]$ m. In the range of thickness considered here, the crack width increases linearly with the layer thickness. Fig. 6 shows the normalized crack w/h measured over a wide range of layer thickness. These measurements are in agreement with the theoretical prediction of eqn (9). The measurements are fitted using the experimentally measured mechanical properties given in Table 1. The evaporation rate is taken to be $V_E = 5 \times 10^{-8}$ m s^{-1} (under drying conditions). The lengthscale $l \sim a$ and the frictional parameter, α, are the two parameters. Best fits lead to: $\alpha_{TM50} = 49.0 \pm 1.9 \times 10^3$ Pa s; $\alpha_{HS40} = 37.4 \pm 0.9 \times 10^3$ Pa s; $\alpha_{SM30} = 10.0 \pm 0.2 \times 10^3$ Pa s. In the case of the silica HS-40 layer, these values well satisfy
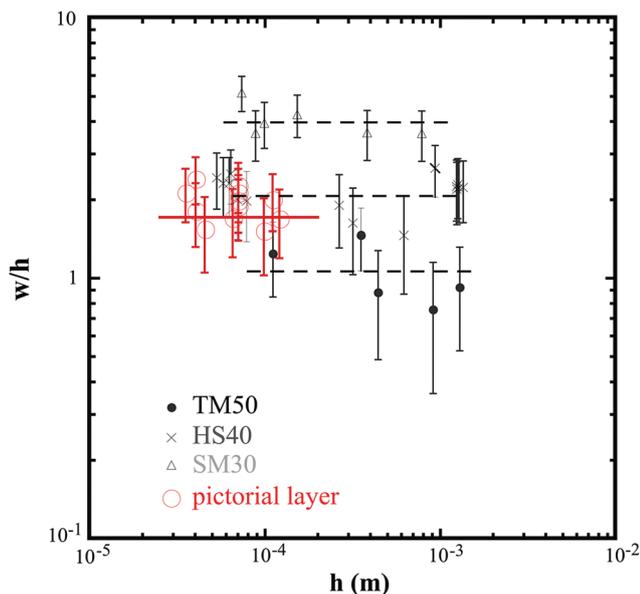
Fig. 6 Dimensionless width, w/h, of cracks of 1st generation $vs.$ layer thickness, h, in a log–log scale. Each dot corresponds to a mean value performed on several cracks. Measurements on model systems and on the pictorial layer of ''Jeanne d'Arc en prison'' by Louis Crignier. The plain lines correspond to a fit with eqn (9) using the parameters σ_Y and E deduced from Fig. 4.

the time variation of the width according to eqn (8) (see the plot in Fig. 5c and direct measurements indicated by circle dots). We have then compared the value deduced from the fit with values obtained in a previous work in delamination experiments.[28] In that paper, it has been shown that the adhesion between the gel and the substrate is due to capillary forces close to the gel/substrate interface. Indeed, there are some air-in-liquid capillary bridges in the vicinity of the substrate which are responsible for the strong attractive interaction. A consequence is that after a duration close to 24 hours, when the solvent is completely removed from the gel, we observe that the layer does not adhere anymore to the substrate. The energy of adhesion is found to be equal to the value of the surface tension of water with air.

Thus, an estimation of α based on the liquid meniscus friction can be proposed as the product of the capillary pressure (γ/a) with the typical drying timescale of a meniscus a/V_E; thus $\alpha \approx \gamma/a(a/V_E) \approx \gamma/V_E \approx 10^5$ Pa s, which is of the order of the values obtained from the fits.

Pictorial layer

Measurements of the crack width in a real painting have been carried out for the painting ''Jeanne d'Arc en prison'' presented in Fig. 1, especially in the region of the shoulder where cracks exhibit large opening which ensures that they are drying cracks. The results are plotted as a function of the layer thickness in Fig. 6. We used for the mechanical properties of the paint, data provided for the blue pigment used by the artist for the shoulder of ''Jeanne d'Arc'': azurite in cold pressed linseed oil.[33] The composition of azurite can nevertheless vary with the

proportion of the pigment, binder, or addition of $CaCO_3$ and consequently, the mechanical parameters can vary with the composition of the paint. Given the complexity of the system, we used values found in ref. 19, for azurite in cold pressed linseed oil for a 7.5 years old material. In this way, the uniaxial tensile stress–strain curve (Fig. 4) allows us to estimate the elastic modulus and the yield point of the material (see Table 1). The experimental results show crack width scaling with the layer thickness. The mechanical properties together with eqn (9) are in agreement with the direct measurements of the crack width as shown in Fig. 6. The viscous friction parameter that fits the data is equal to $\alpha = 1.33 \pm 0.10 \times 10^3$ Pa s. The viscous friction is lower than in the case of the sliding of the silica gel induced by shrinkage. This can be due to the fact that the evaporation rate and the surface tension are not well known and are not well defined.

5 Conclusion

We have conducted drying experiments with colloidal silica suspensions and presented crack opening measurements as a function of the thickness of the drying film. The same measurements have also been carried out on a drying crack pattern on a real painting. Using indentation testing, we have measured the elastic modulus and yield stress for the colloidal systems; for the painting, values reported in the literature are used. We propose a model based on a balance between the drying stress in the layer and the shear friction force with the substrate to deduce a linear relation between the final crack width, w, and the thickness, h, and the mechanical properties of the system. The experimental measurements are well fitted by our model and the viscous friction parameter thus estimated is found to be of the order of capillary pressure during the skrinkage. The present model can therefore be applied to evaluate the yield stress and the elastic modulus of paint layers in art paintings. Inconsistency between these values and those typical from that period could then imply the possibility of a copied painting. This model could therefore be a potential complementary technique for the authentication of art paintings. The ratio of the yield stress and the elastic modulus appears to be a key parameter that determines the properties of the final crack pattern.

Acknowledgements

References

1 F. Giorgiutti-Dauphiné and L. Pauchard, *J. Appl. Phys.*, 2016, **120**, 065107.

2 L. Pauchard, V. Lazarus, B. Abou, K. Sekimoto, G. Aitken and C. Lahanier, *Reflets Phys.*, 2007, **3**, 5–9.

3 S. Bucklow, *Stud. Conserv.*, 1997, **42**, 129–140.

4 P. de Willigen, *A Mathematical Study on Craquelure and other Mechanical Damage in Paintings*, WBBM report Series 42/ MOLART Report Series 2, 1999.

5 L. De Viguerie, PhD thesis, Université Pierre et Marie Curie, Paris VI, 2009.

6 L. Goehring, A. Nakahara, T. Dutta, S. Kitsunezaki and S. Tarafdar, *Desiccation Cracks and their Pattern*, Wiley, 2015.

7 N. Lecocq and N. Vandewalle, *Phys. A*, 2003, **321**, 431–441.

8 E. Brener and V. Marchenko, *JETP Lett.*, 2002, **76**, 211–214.

9 T. Baumberger, C. Caroli and O. Ronsin, *Phys. Rev. Lett.*, 2002, **88**, 075509.

10 S. Bohn, L. Pauchard and Y. Couder, *Phys. Rev. E: Stat., Nonlinear, Soft Matter Phys.*, 2005, **71**(046214), 123–139.

11 M. Biot, *J. Appl. Phys.*, 1941, **12**, 155–164.

12 J. Petit, J. Roire and H. Valot, *Encyclopédie de la peinture*, EREC, 1999, vol. 1.

13 R. Iler, *The Chemistry of Silica: Solubility, Polymerization, Colloid and Surface Properties and Biochemistry of Silica*, Wiley Interscience, 1979.

14 J. Malzbender, J. den Toonder, A. Balkenende and G. de With, *Mater. Sci. Eng., R*, 2002, **36**, 47–103.

15 K. Vanstreels, C. Wu, M. Gonzalez, D. Schneider, D. Gidley, P. Verdonck and M. Baklanov, *Langmuir*, 2013, **29**, 12025–12035.

16 F. Boulogne, L. Pauchard and F. Giorgiutti-Dauphiné, *Oil Gas Sci. Technol.*, 2013, **69**, 397–404.

17 K. Johnson, *Contact Mechanics*, Cambridge University Press, 1985.

18 E. Di Giuseppe, A. Davaille, E. Mittelstaedt and M. François, *Rheol. Acta*, 2012, **51**, 451–465.

19 M. Mecklenburg and C. Tumosa, *Art in Transit: Studies in the Transport of Paintings, National Gallery of Art*, 1991.

20 A. Atkinson and R. Guppy, *J. Mater. Sci.*, 1991, **26**, 3869–3873.

21 J. Hutchinson and Z. Suo, *Adv. Appl. Mech.*, 1991, **29**, 63–191.

22 V. Rigid gels and G. Scherer, *J. Non-Cryst. Solids*, 1987, **92**, 122–144.

23 G. Scherer, *J. Non-Cryst. Solids*, 1989, **109**, 171–182.

24 M. Chekchaki and V. Lazarus, *Transp. Porous Media*, 2013, **100**, 143–157.

25 F. Giorgiutti-Dauphiné and L. Pauchard, *Eur. Phys. J. E: Soft Matter Biol. Phys.*, 2014, **37**, 39.

26 C. J. Brinker and G. Scherer, *Sol-Gel Science: the Physics and Chemistry of Sol Gel Processing*, Academic, San Diego, 1990.

27 M. Smith and J. Sharp, *Langmuir*, 2011, **27**, 8009–8017.

28 L. Pauchard, *Europhys. Lett.*, 2006, **74**, 188–194.

29 L. Goehring, W. Clegg and A. Routh, *Soft Matter*, 2011, **7**, 7984–7987.

30 Y. Xu, G. German, A. Mertz and E. Dufresne, *Soft Matter*, 2013, **9**, 3735–3740.

31 W. Yan, Q. Sun and P. Hodgson, *Mater. Lett.*, 2008, **62**, 2260–2262.

32 L. Goehring, W. Clegg and A. Routh, *Phys. Rev. Lett.*, 2013, **110**, 024301.

33 A. Genty-Vincent, E. Eveno, W. Nowik, G. Bastian, E. Ravaud, I. Cabillic, J. Uziel, N. Lubin-Germain and M. Menu, *Appl. Phys. A: Mater. Sci. Process.*, 2015, **121**, 779–788.